Simultaneous Focused Laser Differential Interferometry and High-Speed Schlieren in a Mach 6 Flow

Brett F. Bathel, Gregory C. Herring, Joshua M. Weisberger, Amanda Chou

NASA Langley Research Center, Hampton, VA 23681, USA

E-mail: brett.f.bathel@nasa.gov

Stephen B. Jones

Analytical Mechanics Associates, Inc., Hampton, VA 23681, USA

Abstract. An instrument is demonstrated that is capable of simultaneous and independent flow density fluctuation measurements over the same line-of-sight by combining two optical techniques: focused laser differential interferometry (FLDI) and high-speed schlieren (HSS). The FLDI instrument measures fluctuations at a single point in the flowfield at 10 MHz, with the resulting signal most sensitive in the region nearest the focal plane of the FLDI laser beam. The HSS instrument acquires images at 20 kHz along the same optical axis as the FLDI beam, but with the resulting signal path averaged over the entire HSS line-of-sight. The introduction of the HSS optics into the FLDI beam path provides two high-quality measurement capabilities in a single system with no degradation of performance relative to stand-alone FLDI or HSS instruments.

Keywords: Focused Laser Differential Interferometry, High Speed Schlieren

1. Introduction

The aeronautics research literature contains many examples of multiple diagnostic techniques used to measure the same flow parameter. This is done to ensure that measured results are accurate and/or to provide measurements of mixed resolution or response (e.g. with schlieren and pressure probes [1], particle image velocimetry (PIV) and molecular tagging velocimetry [2], schlieren and PIV [3], pressure-sensitive paint and pressure probes [4], Mach-Zehnder interferometry and focused laser differential interferometry (FLDI) [5], FLDI and high-speed schlieren (HSS) [6, 7], etc.). Often, the application of different methods does not occur at the same exact spatial location and may not be simultaneous due to instrument or test facility constraints (e.g. two physical probes cannot be used at the same position at the same time). Even some optical techniques cannot be conveniently used simultaneously for the same

off-body regions; thus it is uncommon to see two or more diagnostics used simultaneously to probe the same flow region.

However, some non-intrusive optical methods possess attributes favorable for simultaneous use. Comparison of data acquired from conventional FLDI [8, 9] and multi-point FLDI [10, 11] instruments with HSS visualization has recently been performed to verify shockwave velocity measurement results (details of the schlieren technique can be found in Ref. [12]). In these works, the lines-of-sight of the FLDI and HSS instruments were orthogonal to one another, which may not be practical or possible when measurements are performed in wind tunnel facilities with limited optical access. Examples of the non-simultaneous application of schlieren and FLDI techniques to study flow phenomena can be found in Refs. [6, 7, 13, 14, 15]. Additionally, facility operators may require schlieren visualization as a means of monitoring flow quality, which may otherwise be obscured by the presence of another instrument. In this work, a modified version of the FLDI instrument in [16] is used to demonstrate simultaneous FLDI/HSS density gradient measurements over the same line-of-sight. Simultaneous measurement of freestream density fluctuations with FLDI and pitot probe shock standoff distance with HSS were acquired near the end of a recent wind tunnel calibration test [16] in NASA Langley Research Center's 20-Inch Mach 6 Tunnel. A series of laboratory tests were then performed to verify that the inclusion of the HSS system optical components did not interfere with the FLDI system measurements.

2. Experimental Setup

2.1. Wind Tunnel Test

The work reported in [16] was first performed with a conventional, single-point FLDI instrument shown in Fig. 1a, where the continuous wave laser beam propagated along the optical axis (z-axis), oriented perpendicular to the wind tunnel's freestream flow (x-axis). Details pertaining to the 20-Inch Mach 6 Tunnel facility are found in Ref. [17]. With respect to the tunnel's streamwise x-axis, the conventional single-point FLDI signal was effectively a point measurement with a resolution of $\delta_x \approx 180$ μm in x, $\delta_y \approx 50$ μm in y, and extended over a span, δ_z, of several centimeters about the instrument's focal plane (i.e. wind tunnel centerline). The specific value of the extended span δ_z depended on the f-number of the focusing optics ($f/\#$), laser wavelength (λ_0), and the spatial frequencies of the density disturbances passing through the laser beam (k_ρ) as described in [5, 18, 19]. The signal was sampled at 10 MHz, providing density fluctuation time history and spectra potentially up to the 5 MHz Nyquist frequency limit, although no anti-aliasing filters were used in this setup.

After performing measurements reported in Ref. [16] with the conventional single-point FLDI instrument upstream of physical pressure probes without schlieren, a colinear HSS capability was then added to the FLDI setup, shown schematically in Fig. 1b. Note that for this configuration, the FLDI laser propagated from the transmitter to receiver side of the instrument while light from the HSS was counter-propagating. This was done to minimize the light interference between instruments. The HSS-portion of the instrument used a blue LED

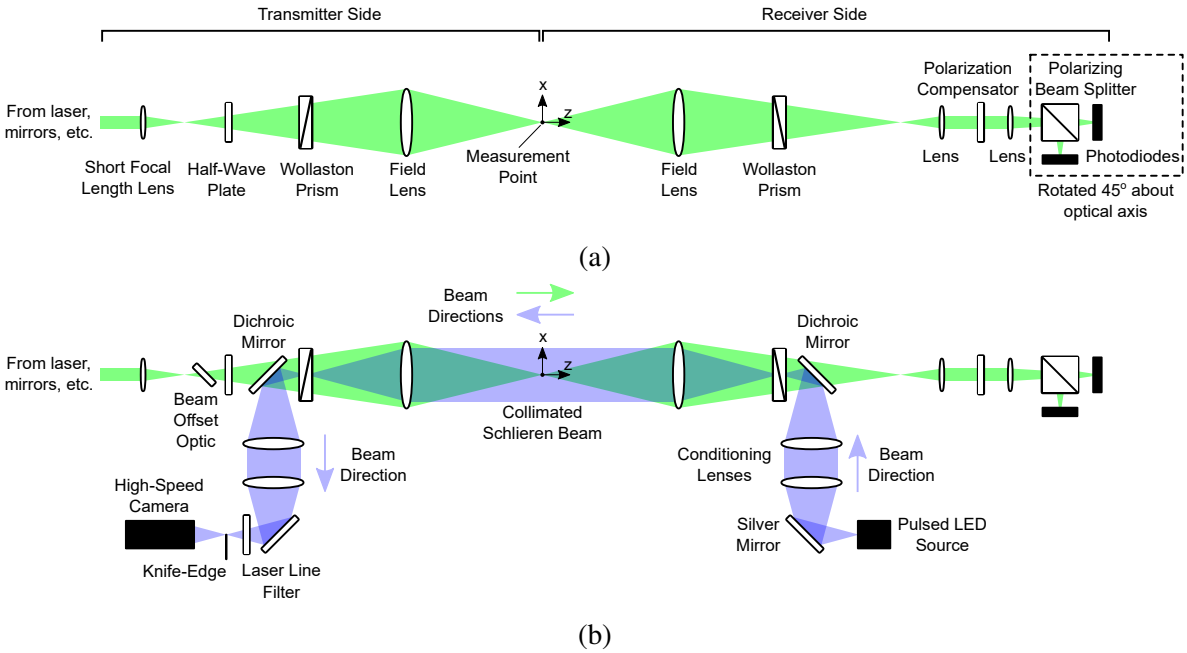

Figure 1: (a) Conventional single-point FLDI instrument and (b) combined single-point FLDI instrument with colinear schlieren system.

(Luminus, PT-120-B) driven by a pulsed laser diode driver (PicoLAS, LDP-V 240-100 V3) in a manner similar to that described by Willert *et al.* [20, 21]. The LED had a center wavelength of $\lambda_{\text{LED}} = 460 \pm 10$ nm and was pulsed at 20 kHz with a pulse width of $\Delta t_{\text{LED}} \approx 0.7$ μs. A one-to-one imaging lens (Thorlabs, MAP104040-A) was placed in front of the LED's active surface and was enclosed within the pulsed LED source housing. This lens imaged the LED light onto an adjustable aperture that was used to control the diameter of the point source (typically 1-2 mm). An imaging periscope, consisting of a silvered mirror oriented at 45° relative to the FLDI instrument's optical axis (Thorlabs, PF20-03-P01), two achromat conditioning lenses, and a 50-mm-diameter dichroic long-pass mirror with a 490 nm cutoff also oriented at 45° relative to the FLDI instrument's optical axis (Thorlabs, DMLP490L), was mounted on both the transmitter and receiver sides of the instrument as shown in Fig. 1b. The dichroic mirrors were used to couple the blue LED light into, and out of, the optical path used for the green 532 nm laser beam of the FLDI instrument. The placement of these dichroic mirrors ensured that they did not clip the transmitted FLDI beam and that they did not affect the alignment between the Wollaston prisms and field lenses. The periscope on the receiver side of the instrument re-imaged the point source at one focal length from the field lens, corresponding to the location of the receiver-side Wollaston prism. The receiver-side field lens then collimated the blue light which was passed through the test section.

On the transmitter-side, the counter-propagating blue collimated schlieren beam was focused by the field lens onto the Wollaston prism and subsequently coupled out of the FLDI instrument by the periscope. A transparent beam offset optic (Thorlabs, BCP4210) was used in the FLDI beam path to compensate for the refractive offset imparted by the periscope's

dichroic mirror. As the light from the periscope was imaged to a focused spot, it was passed through a laser line notch filter (Thorlabs, NF533-17) to block any scattered FLDI laser light. A knife edge oriented perpendicular to the floor of the rectangular-shaped test section was used to spatially filter blue light at its focus. An f/2, 105-mm focal length lens (Nikon, #1932) then re-imaged the spatially-filtered light onto a high-speed camera (Photron, SA-Z 2100K), which acquired 1024×1024-pixel images at 20 kHz, with 48 μs exposures centered on the LED pulses. These images show the path-integrated density gradient signal over the entire width of the test section, including tunnel wall boundary layers.

2.2. Laboratory Test

A laboratory test was also performed to show that the addition of the HSS optics (periscopes and beam offset optic) and pulsed LED do not affect the FLDI signal. For this test, modified versions of the instruments shown in Fig. 1 were constructed. For these laboratory instruments, a quarter-wave plate (Thorlabs, WPQ10M-532) was used in place of the Berek's variable-wave plate (Newport, 5540) as the polarization compensator, and a linear polarizer (Thorlabs, LPVISA100-MP2) was installed just after this quarter-wave plate. A non-polarizing beam-splitter (Thorlabs, CCM1-BS013) was then installed in place of the polarizing beam-splitter, and one of the two photodiodes replaced with a CMOS camera (Basler, acA1920-150um) to aid in alignment of the beam on the remaining photodiode (Thorlabs, DET36A). A 550-nm long-pass filter (Thorlabs, FGL550M) and neutral density filter (Thorlabs, ND40A) were mounted to the front of the camera to better image the beam. As in the wind tunnel test, the half-wave plate was used to balance the transmitted intensity of the FLDI beams initially split by the transmitter-side Wollaston prism. The polarization compensator and linear polarizer were then adjusted such that the intensity of the beam incident on the photodiode corresponded to the middle of the interference fringe. The laser power was also adjusted to approximately match the power incident on the photodiode when the HSS optics were not present. The signal was sampled at 12.5 MHz and again no anti-aliasing filters were used. Finally, an sCMOS camera with a 105 mm lens (Nikon, #1932) and 500 mm lens (Thorlabs, AC508-500-A) in series were used in place of the high-speed camera to acquire schlieren images of an air jet issuing from a small-diameter (inner diameter of 1.2 mm) stainless steel tube.

3. Results and Discussion

3.1. Wind Tunnel Test

For the wind tunnel test, the HSS field-of-view of the combined FLDI/HSS system described in Sec. 2.1 was trained upon two $d_{\text{probe}} = 4.4$-mm-diameter pitot pressure probes (PCB, 132-A31) in order to capture the shock standoff distance, Δx_{BS}. While the HSS images were obtained with a 48 μs exposure, the flow appeared frozen as the $\Delta t_{\text{LED}} \approx 0.7$ μs LED illumination pulse served as the camera's effective exposure. Figure 2 shows sample HSS results with Figs. 2a and 2b representing 250-image-averages of the flow about the probes

with unperturbed, smooth symmetric shocks acquired at facility unit Reynolds numbers, $\mathrm{Re_x}$, of 3.4×10^6 m^{-1} and 26.3×10^6 m^{-1}, respectively. Here, the center of the FLDI measurement point is denoted by the green marker (not to scale) with the size of the underlying white box corresponding to the uncertainty in this measurement position. For both $\mathrm{Re_x}$ conditions, a value of $\Delta x_{\mathrm{BS}} = 1.1\pm0.2$ mm was measured, giving $\Delta x_{\mathrm{BS}}/d_{\mathrm{probe}} = 0.25$, which is in agreement with experimental data for a body of revolution with a flat nose at Mach 6 in Ref. [22]. Figure 2c shows a single exposure with a perturbed shock on the lower probe at $\mathrm{Re_x} = 26.3\times10^6$ m^{-1}, where the short LED pulse coincided, by chance, with a probable rare particle strike on the lower probe. Unfortunately, FLDI acquisition was not enabled at the instant this event occurred. These images demonstrate that HSS data can be acquired with remarkably high quality even when coupled into an FLDI system using the methods described in this work.

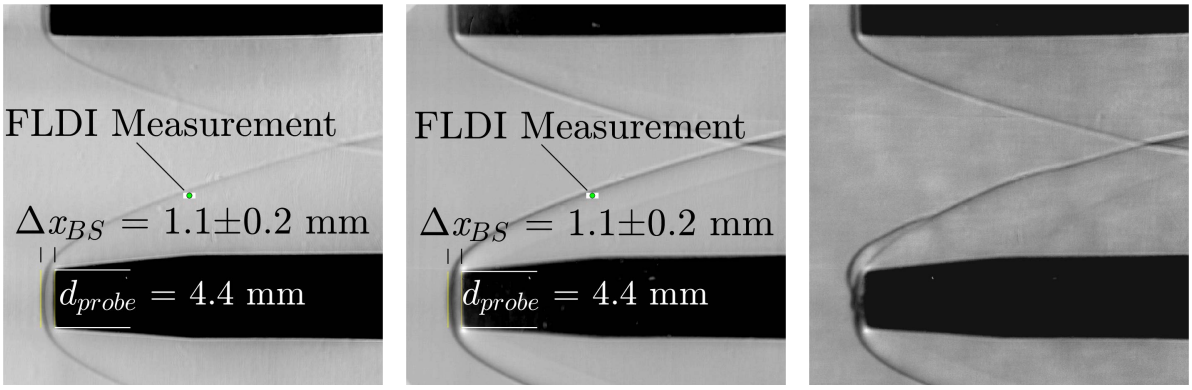

(a) (b) (c)

Figure 2: Time-averaged images of pressure probes in Mach 6 freestream flow for $\mathrm{Re_x}$ of (a) 3.4×10^6 m^{-1} and (b) 26.3×10^6 m^{-1}, and (c) single-shot image of probable particle strike at $\mathrm{Re_x} = 26.3\times10^6$ m^{-1}. The green point denoting the FLDI measurement location is not to scale.

Figure 3 shows a three second segment of the temporal history of the probe-measured pressure fluctuations at $\mathrm{Re_x} = 26.3\times10^6$ m^{-1}. Here, the red and blue data correspond to the pressure signals from the upper and lower probes shown in the HSS images in Fig. 2, respectively. In this figure, the dashed black box highlights the probable particle strike observed in Fig. 2c, with the inset plot revealing the short transient perturbation in the voltage signal. Note that the pressure signal during this event exceeded the dynamic range of the data acquisition system, resulting in flat peaks near ±11 kPa. Without the HSS capability, it would have been difficult to reliably determine the cause of the probe signal voltage transient. The two adjacent frames, before and after this strike, showed no sign of the shock perturbation; thus, the duration of the shock perturbation was less than ≈100 μs, which is similar to the duration of the short (200 μs) transient perturbation in the inset plot of Fig. 3. No other instance of such a perturbation was observed in the HSS data throughout the test.

While the colinear HSS images were of high quality, it remained to be determined

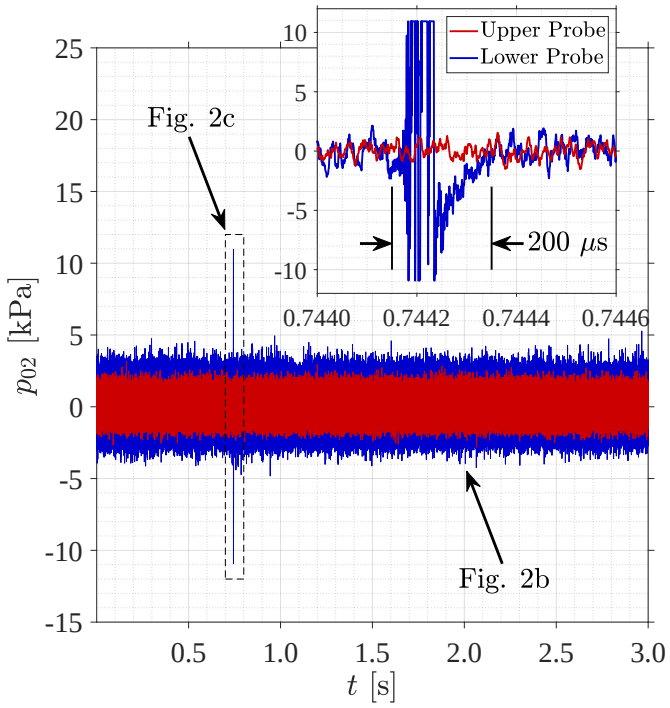

Figure 3: Pressure probe signals from upper (red) and lower (blue) probes shown in Fig. 2 for $\mathrm{Re_x} = 26.3\times10^6$ m^{-1}. Inset plot shows short, transient probable particle strike corresponding to dashed box.

whether the presence of the beam offset optic, the two dichroic mirrors in the FLDI optical path, and the pulsed LED light source adversely affected the FLDI measurements. Figure 4 shows sample FLDI power spectral density (PSD) estimates of broadband density fluctuations obtained from different tunnel runs for two different $\mathrm{Re_x}$ conditions. Run data denoted as 'No HSS' were taken without the HSS optics installed, gave reproducible spectral data (nearly entirely overlapping), and were taken at a freestream location 139.7 mm upstream of the FLDI measurement location shown in Fig. 2. Run data denoted as 'HSS' were taken with the HSS optics installed, at a location just behind the probe shock, and with the HSS in operation. Although it was not optimum to change two experimental parameters at the same time (instrument configuration and position of the measurement points) the FLDI/HSS work was a secondary measurement on the higher-priority tunnel calibration work [16] which required the change of location for the two measurements. The small differences in spectral amplitude for runs with and without the HSS system installed and operating in Fig. 4 are most likely due to the different flow conditions that exist between freestream versus post-shock flow. While it was thought that the presence of the HSS system (optics and LED operation) did not influence the FLDI spectra, the data of Fig. 4 alone were not sufficient to confidently rule out such a possibility.

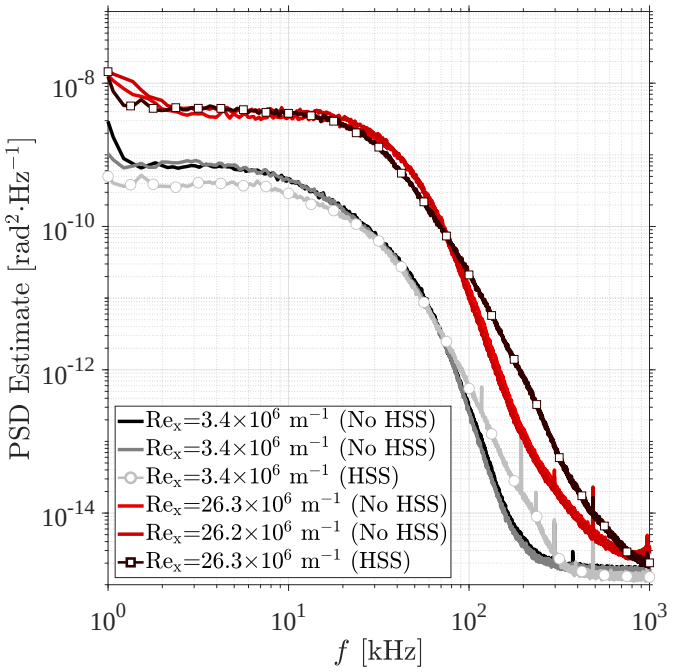

Figure 4: FLDI spectra for freestream Re_x conditions of 3.4×10^6 m^{-1} and 26.3×10^6 m^{-1} both with and without the HSS system present.

3.2. Laboratory Test

In order to rule out the possibility of the HSS system having any influence on the shape of the measured FLDI spectra, a separate set of laboratory measurements were obtained using a conventional single-point FLDI similar to that shown in Fig. 1a and a combined FLDI/HSS system similar to that shown in Fig. 1b, but with the modifications described in Sec. 2.2. Figure 5 shows a sample single-shot schlieren image of the laboratory air jet obtained with the modified FLDI/HSS system as well as the approximate location of the FLDI measurement point. For these measurements, the FLDI measurement point was positioned in a region of the jet flow that exhibited a broad noise spectrum extending out to 1 MHz. In this test, FLDI spectra were first obtained with the conventional single-point FLDI system both with and without the air jet flowing. The HSS optics were then installed and FLDI spectra again obtained both with and without the air jet flowing.

Figure 6 shows the FLDI spectra obtained with the conventional FLDI system and combined FLDI/HSS system. For the tests with the air jet flowing, the spectrum obtained with the HSS optics in place, but without the LED in operation (solid gray curve, circular markers), had no discernible differences from the spectrum obtained with the conventional FLDI system (solid black curve). Baseline results obtained with the air jet off and without the LED in operation for both the conventional FLDI system (dashed black curve) and combined FLDI/HSS system (dashed gray curve, square markers) were also obtained and again the shapes of the PSD spectra did not appear to be influenced by the presence of the HSS

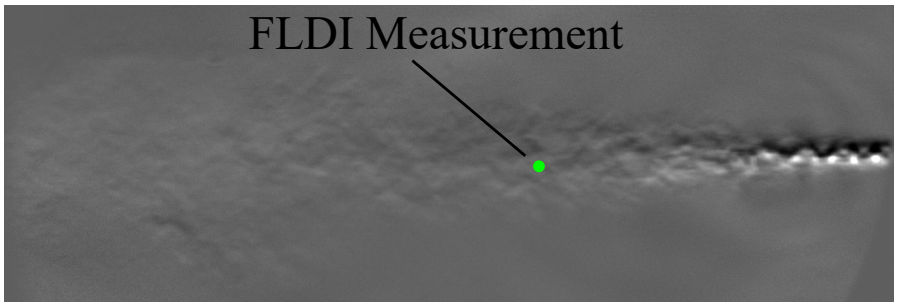

Figure 5: Single-shot schlieren image of laboratory jet flow. The green point denoting FLDI measurement location is not to scale.

optics. Finally, when the blue LED was operated at 20 kHz, only small amplitude electrical noise spikes were observed in the measured spectra (solid blue curve), with peak magnitudes well below that of the electrical noise spikes observed in the baseline spectra without LED operation. The results of this test show that the presence of the HSS optics and operation of the pulsed LED source in the wind tunnel test did not influence the shape of the measured FLDI spectra, and that the observed differences are most likely a result of differing flow properties, as suspected.

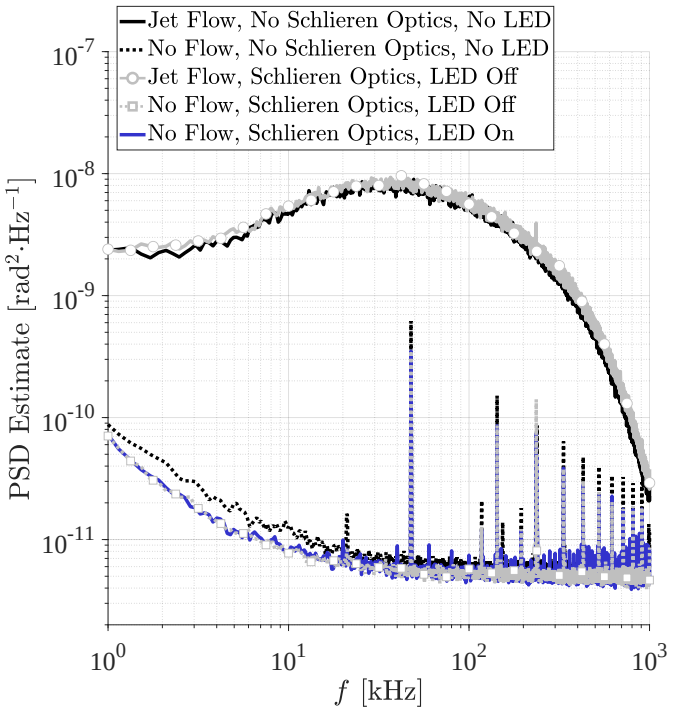

Figure 6: FLDI spectra for jet flow with (gray, circular markers) and without (solid black) HSS system present. No flow FLDI spectra shown with (blue) and without (dashed gray, square markers) LED operation with HSS system present. Baseline no flow FLDI spectra without HSS system present and no LED operation shown for reference (dashed black).

3.3. Schlieren Alignment, Sensitivity, and Alternative Configurations

The relatively high-quality (intensity uniformity, spatial resolution, and temporal resolution) schlieren images obtained with the setup described in this work required careful alignment of the optics within the two HSS periscopes as well as the alignment of these optics to the two field lenses on the transmitter and receiver sides of the instrument. To facilitate alignment, it is recommended that the components of a combined FLDI/HSS instrument be mounted in an optical cage mounting system. Further, both the silvered mirrors and dichroic mirrors shown in Fig. 1b should be placed in kinematic mounts for ease of adjustability and the LED should be placed on a three-axis stage. Finally, the conditioning lenses in the periscopes should be mounted in adjustable *x*-*y* translation mounts to achieve optimal alignment. As the HSS system is brought into alignment, the sensitivity in the schlieren images should be such that room air currents passing through the field-of-view become visible. While not attempted in this work, future work will focus on achieving the precise alignment needed to obtain interferometric schlieren-like images by making use of the Wollaston prisms, similar to the results obtained in Refs. [23, 24, 25, 26].

4. Conclusions

Simultaneous density fluctuation measurements have been demonstrated over the same spatial region using two optical techniques: FLDI and HSS. The combined FLDI/HSS instrument configuration allowed for the acquisition of mixed frequency and spatial resolution measurements of density fluctuations, providing simultaneous MHz-rate point (FLDI) and high-speed 2D path-integrated visualization (HSS) capabilities. In this work, the FLDI measurements were used to assess the spectral characteristics of the flow while the HSS was used to determine the shock standoff distance in front of pressure probes. The HSS was also used to visualize a probable particle strike on one of the pressure probes. Confidently attributing the cause of the transient signal spike in the pressure probe data would have been difficult without the capability of optical methods (HSS in this case). Simultaneous use of these noninvasive diagnostics can increase the amount of data collected and greatly improve aeronautics researchers' confidence in the overall validity of the reported results, compared to the use of only a single method. As was demonstrated in this work, the simultaneous measurement capability was also provided without degradation in the data from each instrument. Finally, laboratory tests demonstrated that the presence and operation of the HSS system does not interfere with the FLDI measurement capability.

Acknowledgments

This work was supported by the Hypersonics Technology Project (HTP), the Aeronautics Evaluation and Test Capabilities (AETC) project, and the Transformational Tools and Technologies (TTT) project. The authors would like to thank Larson Stacey, Kevin Hollingsworth, Grace Gleason, Johnny Ellis, and Jonathan Crider for their assistance with

wind tunnel testing. The authors would also like to thank the reviewers for their comments as they improved the overall quality of the paper.

References

[1] S. J. Laurence, A. Wagner, and K. Hannemann. Schlieren-based techniques for investigating instability development and transition in a hypersonic boundary layer. *Experiments in Fluids*, 55(8), July 2014.

[2] Matthieu Andre, Philippe Bardet, Ross A. Burns, and Paul M. Danehy. Development of Hydroxyl Tagging Velocimetry for Low Velocity Flows. In *32nd AIAA Aerodynamic Measurement Technology and Ground Testing Conference*. American Institute of Aeronautics and Astronautics, June 2016. Paper 2016-3247.

[3] Dennis R. Jonassen, Gary S. Settles, and Michael D. Tronosky. Schlieren "PIV" for turbulent flows. *Optics and Lasers in Engineering*, 44(3-4):190–207, March 2006.

[4] Nettie Roozeboom, Jessica Powell, Jennifer Baerny, David Murakami, Christina Ngo, Theodore J. Garbeff, James C. Ross, and Ross Flach. Development of Unsteady Pressure-Sensitive Paint Application on NASA Space Launch System. In *2019 AIAA Aviation Forum*. American Institute of Aeronautics and Astronautics, June 2019. Paper 2019-3502.

[5] J.M. Lawson, M.C. Neet, I.J. Grossman, and J.M. Austin. Static and dynamic characterization of a focused laser differential interferometer. *Experiments in Fluids*, 61(8):1–11, 2020.

[6] Tim P. Wadhams, Matthew MacLean, Ron Parker, and Michael Holden. Sharp Cone Boundary Layer Transition and Stability at Mach 10. In *22nd AIAA International Space Planes and Hypersonics Systems and Technologies Conference*. American Institute of Aeronautics and Astronautics, September 2018. Paper 2018-5323.

[7] Theron J. Price, Mark Gragston, John D. Schmisseur, and Phillip A. Kreth. Measurement of supersonic jet screech with focused laser differential interferometry. *Applied Optics*, 59(28):8902, September 2020.

[8] Joshua Weisberger, Brett F. Bathel, Stephen B. Jones, and Gregory C. Herring. Focused Laser Differential Interferometry Measurements at NASA Langley 20-Inch Mach 6. In *AIAA Aviation 2019 Forum*. American Institute of Aeronautics and Astronautics, June 2019. Paper 2019-2903.

[9] Brett F. Bathel, Joshua M. Weisberger, Gregory C. Herring, Rudolph A. King, Stephen B. Jones, Richard E. Kennedy, and Stuart J. Laurence. Two-point, parallel-beam focused laser differential interferometry with a Nomarski prism. *Applied Optics*, 59(2):244, January 2020.

[10] Joshua M. Weisberger, Brett F. Bathel, Gregory C. Herring, Gregory M. Buck, Stephen B. Jones, and Angelo A. Cavone. Multi-point line focused laser differential interferometer for high-speed flow fluctuation measurements. *Applied Optics*, 59(35):11180, December 2020.

[11] Joshua M. Weisberger, Brett F. Bathel, Gregory C. Herring, Gregory M. Buck, Stephen B. Jones, and Angelo A. Cavone. Two-Line Focused Laser Differential Interferometry of a Flat Plate Boundary Layer at Mach 6. In *2021 AIAA Scitech Forum*. American Institute of Aeronautics and Astronautics, January 2021. Paper 2021-0601.

[12] Gary S. Settles. *Schlieren and Shadowgraph Techniques: Visualizing Phenomena in Transparent Media*. Springer Berlin Heidelberg, 2006.

[13] Andrew Ceruzzi, Braeden Callis, Daniel Weber, and Christopher P. Cadou. Application of Focused Laser Differential Interferometry (FLDI) in a Supersonic Boundary Layer. In *AIAA Scitech 2020 Forum*. American Institute of Aeronautics and Astronautics, January 2020. Paper 2020-1973.

[14] Nick Parziale, Joseph Shepherd, and Hans Hornung. Differential Interferometric Measurement of Instability at Two Points in a Hypervelocity Boundary Layer. In *51st AIAA Aerospace Sciences Meeting*. American Institute of Aeronautics and Astronautics, January 2013. Paper 2013-521.

[15] B. E. Schmidt and J. E. Shepherd. Analysis of focused laser differential interferometry. *Applied Optics*, 54(28):8459, September 2015.

[16] Amanda Chou, Andrew Leidy, Rudolph A. King, Brett F. Bathel, and Gregory Herring. Measurements of Freestream Fluctuations in the NASA Langley 20-Inch Mach 6 Tunnel. In *2018 AIAA Fluid Dynamics Conference*. American Institute of Aeronautics and Astronautics, June 2018. Paper 2018-3073.

[17] Karen T. Berger, Kevin E. Hollingsworth, Shelia A. Wright, and Shann J. Rufer. NASA Langley Aerothermodynamics Laboratory: Hypersonic Testing Capabilities. In *53rd AIAA Aerospace Sciences Meeting*. American Institute of Aeronautics and Astronautics, January 2015. Paper 2015-1337.

[18] N. J. Parziale, J. E. Shepherd, and H. G. Hornung. Differential Interferometric Measurement of Instability in a Hypervelocity Boundary Layer. *AIAA Journal*, 51(3):750–754, March 2013.

[19] Gary S. Settles and Matthew R. Fulghum. The focusing laser differential interferometer, an instrument for localized turbulence measurements in refractive flows. *Journal of Fluids Engineering*, 138(10), July 2016.

[20] C. Willert, B. Stasicki, J. Klinner, and S. Moessner. Pulsed operation of high-power light emitting diodes for imaging flow velocimetry. *Measurement Science and Technology*, 21(7), June 2010.

[21] Christian E. Willert, Daniel M. Mitchell, and Julio Soria. An assessment of high-power light-emitting diodes for high frame rate schlieren imaging. *Experiments in Fluids*, 53(2):413–421, April 2012.

[22] H. W. Liepmann and A. Roshko. *Elements of Gas Dynamics*. Dover Publications Inc., 2002. pp. 104–105.

[23] W. F. Merzkirch. A Simple Schlieren Interferometer System. *AIAA Journal*, 3(10):1974–1976, October 1965.

[24] R. D. Small, V. A. Sernas, and R. H. Page. Single Beam Schlieren Interferometer Using a Wollaston Prism. *Applied Optics*, 11(4):858–862, April 1972.

[25] H. Oertel and K. Bühler. A special differential interferometer used for heat convection investigations. *International Journal of Heat and Mass Transfer*, 21(8):1111–1115, August 1978.

[26] Matthew M. Biss, Gary S. Settles, Matthew E. Staymates, and Simon R. Sanderson. Differential schlieren-interferometry with a simple adjustable Wollaston-like prism. *Applied Optics*, 47(3):328–335, January 2008.